CHAPTER I

General Properties of Particles and Radiation

1. Introduction

The main concern of high-energy physics is with the properties of matter and space at distances of the order of 10^{-13} cm (the classical electron radius) or smaller. The investigation of these properties is intimately concerned with the "structure" and interactions of the fundamental particles which are listed in Table I.[1]

To produce most of these particles (the exceptions being the neutrino, electron, positron, proton, and neutron), high-energy accelerators are required capable of supplying the necessary rest mass in the form of energy. In addition, except in rare instances, the uncertainty principle demands that momenta in excess of 150 Mev/c must be used if interest is centered on distances of 10^{-13} cm or less.

During the last few years a formidable range of techniques has become available for making measurements with the large accelerators. Such measurements consist in general of two parts: characterization of the particles under investigation (in a few instances this is trivial; for instance the circulating beam in a proton synchrotron is composed entirely of protons), and the following out of the subsequent histories of the particles. Intimately connected with such measurements are certain basic properties and laws such as deflection in electric and magnetic fields and ionization.

The techniques used for measurement are divided into two different types. Visual techniques employ cloud chambers, diffusion chambers, emulsion, bubble chambers, and other devices in which everything is recorded photographically. The desired information is later extracted and measured by visual inspection. The second class of techniques employs electronic methods of identifying particles, and the required information, in the form of electronic pulses, is usually extracted by electronic sorting. In the future, photographs may be made with a television camera and the image stored on magnetic tape for subsequent electronic analysis.

However, the characteristic properties of the particles are common to the various techniques and are summarized in Table II.

The subsequent sections of this chapter deal in detail with these

Table I. Masses and Mean Lives on Elementary Particles[a]

Particle	Spin	Mass, Mev[b]	Mean life, sec
Photon	1	0	Stable
Neutrino	$\frac{1}{2}$	0	Stable
Leptons, e^-, e^+	$\frac{1}{2}$	0.510976	Stable
μ^-, μ^+	$\frac{1}{2}$	105.70 ± 0.06	$(2.22 \pm 0.02) \times 10^{-6}$
Mesons, π^-, π^+	0	139.63 ± 0.06	$(2.56 \pm 0.05) \times 10^{-8}$
π^0	0	135.01 ± 0.16	$(0.0 + 0.4) \times 10^{-15}$
K^-, K^+	0	494.0 ± 0.2	$(1.221 \pm 0.013) \times 10^{-8}$
K^0	0	498.8 − 1.1	K_1: $(0.95 \pm 0.08) \times 10^{-10}$ K_2: $\sim 6 \times 10^{-8}$
p	$\frac{1}{2}$	938.213 ± 0.01	Stable
n	$\frac{1}{2}$	939.506 ± 0.01	$(1.04 \pm 0.13) \times 10^{3}$
Λ^0	$\frac{1}{2}$	1115.2 ± 0.14	$(2.77 \pm 0.15) \times 10^{-10}$
Σ^+	$\frac{1}{2}$	1189.4 ± 0.25	$(0.78 \pm 0.074) \times 10^{-10}$
Σ^-	$\frac{1}{2}$	1196.5 ± 0.5	$(1.67 \pm 0.17) \times 10^{-10}$
Σ^0	$\frac{1}{2}$	1190 (+1.2, −2.0)	Theoretically 10^{-19}
Ξ	?	1320.4 ± 2.2	$(1.9 \pm 0.5) \times 10^{-10}$
Ξ^0	?	1311 ± 8	$(1.5) \times 10^{-10}$ (one event)

[a] From reference 10.

[b] Errors represent standard deviation.

characteristics and also with properties specific to electrons, γ-rays, and neutrons.

2. Interaction with the Electromagnetic Field

2.1. *Curvature in a Magnetic Field*

One of the most convenient methods of measurement uses a magnetic deflection, either to prepare a beam of particles with a given momentum or to measure the momentum. The formula for the radius of curvature ρ of a charged particle in a magnetic field is given by the standard electromagnetic formula

$$\rho_{\text{cm}} = \frac{P_{\text{Mev}/c} \times 3.333 \times 10^{2}}{zH} \tag{1}$$

where H is in gauss, P in Mev/c, ρ in cm, and z is the charge of the particle.

Figures 1, 2, and 3 show values of momentum P, β (v/c), and kinetic energy E in units of the rest mass M.

Table II. Characteristic Experimental Properties of Particles[a]

Property measured	Property is a function of	Comments
	Interaction with electromagnetic field	
Curvature in magnetic field	$\frac{p}{z}$	Simple and widely used
Curvature in electric field	$\frac{\beta}{p_z}$	Limited application due to necessity for high field gradients
	Interaction with the Coulomb field of nuclei	
Ionization	z, β	Widely used
Production of "knock-on" electrons	z, β	Application limited to high z particles
Range	z, β	Widely used for low-energy particles
Multiple scattering	$z, p\beta$	Widely used with "visual" techniques when magnetic curvature is unavailable
	Kinematic methods	
Elastic collisions with protons	Mass and energy	Useful for neutral particles as well as charged
Decay products and correlation angles	Mass or ratio of masses	Useful for neutral particles as well as charged
	Interaction with media	
Cerenkov radiation	z, β	Only used in Cerenkov counters
	Special electronic methods	
Time-of-flight between two points	v	Wide application
Total energy loss	E	Data must be obtained with large counters which may limit applications

[a] p is the momentum, z the charge of the particle, β the ratio of the velocity to the velocity of light, v the velocity, and E the energy.

2.2. *Curvature in an Electric Field*

Electric fields are not used extensively to deflect particles owing to the high field gradients required to give a reasonable beam deflec-

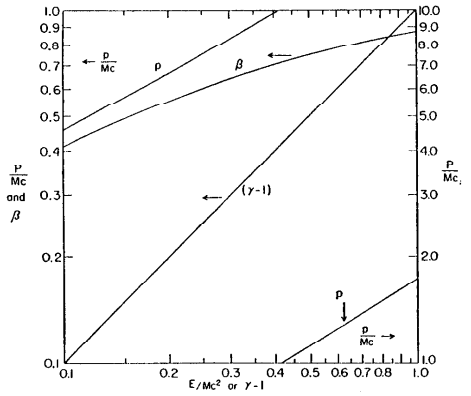

Fig. 1. Momentum, kinetic energy, and β as a function of kinetic energy (all in units of the rest mass).

tion. However, a combination of a magnetic channel, selecting a given momentum, followed by an electric field acts as an efficient mass spectrometer and is likely to find increasing application. This in fact was the classic method used by J. J. Thompson in measuring the mass of the electron. The curvature in an electric field E is given by

$$\rho_{cm} = \frac{10^6 P_{Mev/c}\beta}{ZE_{volts/cm}} \tag{2}$$

For $\beta \sim 1$, the electric field in volts/cm has to be roughly three hundred times larger than a magnetic field in gauss to give an equivalent deflection.

3. Coulomb Scattering by Nuclei

Besides the application of external fields, the strong internal fields in matter can be used to provide measurable deflections. A charged particle traversing any medium encounters large field gradients of the order of 10^8 volts/cm, owing to the nuclear charges. These gradients cause "Coulomb scattering."

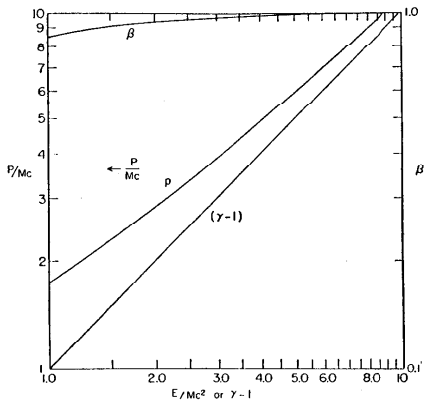

Fig. 2. Momentum, kinetic energy, and β as a function of kinetic energy (all in units of the rest mass).

A few general remarks can be made about the orders of magnitude involved in Coulomb scattering.[31] If the velocity of the incident particle is v, and its distance of closest approach to a nucleus of charge Z is r (r is the impact parameter), then a force of the zZe^2/r^2 acts for a time $\sim r/v$, and thus the momentum change Δp is $\sim zZe^2/rv$. Such a description is meaningful from the viewpoint of the Heisenberg uncertainty principle if the uncertainty in the position of the particle relative to the nucleus is less than r. The condition for the classical approach outlined above, as opposed to a quantal description, is that the uncertainty in position Δr is less than r, or

$$\Delta r \approx \frac{\hbar}{\Delta p} < r \tag{3}$$

which is equivalent to

$$\frac{zZe^2}{\hbar c\beta} > 1 \tag{4}$$

If the condition given by Eq. (4) holds, classical mechanics

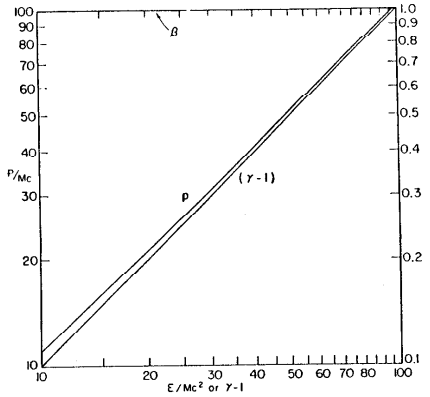

Fig. 3. Momentum, kinetic energy, and β as a function of kinetic energy (all in units of the rest mass).

can be used with approximate validity. The maximum angle of scattering θ_{max} for a nucleus of radius r_{min} is given by

$$\theta_{max} \approx \frac{\Delta p_{max}}{p} \approx \frac{zZe^2}{r_{min} m v^2} \tag{5}$$

If condition (4) is invalid, a wave mechanical description must be used.

In a wave mechanical description, if the incident wave is not appreciably perturbed as it approaches the nucleus, the angle of deflection corresponding to a given impact parameter r is $\theta \approx \lambda/r$. This result is simply the angle for diffraction of a wave of wavelength λ by an object of size r. Hence the maximum angle of deflection θ_{max} is λ/r_{min} and the minimum angle $\theta_{min} = \lambda/r_{max}$.

An accurate solution of the wave mechanical problem shows that the condition for validity of the assumption of small perturbation of the incident wave is

$$\frac{zZe^2}{hc\beta} < 1 \tag{6}$$

Table III. Table of Coulomb Scattering for Particles of Different Spins[a]

Spin	Magnetic moment, units $eh/2Mc$	Scattering in units of $z^2Z^2e^4/p^2\beta^2c^2 \times \mathrm{cosec}^4 \frac{1}{2}\theta$
0	0	1
$\frac{1}{2}$	1	$1 - \beta^2 \sin^2 \frac{1}{2}\theta$
$\frac{1}{2}$	$\mu \geqq 1$	$(\mu - 1)^2 \sin^2 \frac{1}{2}\theta$ for $\gamma \gg 1$
1	1	$1 + \frac{\beta^4}{6(1-\beta^2)} \sin^2 \frac{1}{2}\theta$
1	$\mu \geqq 1$	$\frac{4(\mu-1)^2 \sin^2 \frac{1}{2}\theta}{3} \quad 1 - \beta^2$

[a] From reference 19.

For both the classical and quantal cases, the formula for the differential scattering cross section $\sigma(\theta)$ per steradian is given for small energies as[17]

$$\sigma(\theta)\, d\Omega = \frac{z^2Z^2e^4}{4p^2\beta^2c^2} \mathrm{cosec}^4 \tfrac{1}{2}\theta \, d\Omega \tag{7}$$

which can be rewritten as

$$\sigma(\theta)\, d\Omega = 5.19 \frac{z^2Z^2}{(p_{\mathrm{Mev}/c}\beta)^2} \mathrm{cosec}^4 \tfrac{1}{2}\theta \, d\Omega \text{ mb/steradian} \tag{8}$$

where $p\beta$ is in Mev/c and $\sigma(\theta)$ is the cross section in units of 10^{-27} cm^2 per steradian.

At relativistic energies small corrections must be made for particles with spin (Table III).

For the case of electrons scattered by the Coulomb field the cross section is changed by the factor $(1 - \beta^2 \sin^2 \frac{1}{2}\theta)$. Table III gives the appropriate cross sections.

4. Multiple Coulomb Scattering

On traversing a block of material, a particle suffers a large number of small Coulomb deflections. The additive effect of a large number of such small collisions constitutes multiple Coulomb scattering. The rms value of a large number of random small deflections can be found by Gaussian addition[30] and is given by

$$\langle \theta^2 \rangle_{av} = \int_0^\infty \theta^2 I'(\theta)\, d\theta \tag{9}$$

where $I'(\theta)\ d\theta$ is the number of collisions in an angular interval from θ to $\theta + d\theta$.

$I'(\theta)$ can be derived from Eq. (6) by approximating $\sin\theta$ as θ:

$$I'(\theta) = 8\pi \sum_i \frac{N_i Z_i^2}{(p\beta c)^2} z^2 e^4 x \frac{d\theta}{\theta^3} \tag{10}$$

where N_i is the number of atoms of charge Z_i per gram and x is the thickness of matter traversed in g/cm^2. Integrating $I'(\theta)$ from θ_{max} to θ_{min} gives

$$\langle\theta^2\rangle_{av} = \int_{\theta_{min}}^{\theta_{max}} \theta^2 I'(\theta)\ d\theta \tag{11}$$

$$= 8\pi \sum_i \frac{(N_i Z_i^2) z^2 e^4 x}{(p\beta c)^2} \int_{\theta_{min}}^{\theta_{max}} \frac{d\theta}{\theta} \tag{12}$$

From the discussion of Section 3

$$\frac{\theta_{max}}{\theta_{min}} \approx \frac{r_{max}}{r_{min}} \tag{13}$$

and hence

$$\langle\theta^2\rangle_{av} = 16\pi \sum_i \frac{(N_i Z_i^{\ 2}) z^2 e^4 x}{(p\beta c)^2} \log_e \left(\frac{r_{max}}{r_{min}}\right)^{1/2} \tag{14}$$

Here r_{min} is approximately the radius of the nucleus and is given by $r_{min} \approx A^{1/3}\ 1.20 \times 10^{-13}$ cm.

From the Thomas-Fermi model of the atom has been derived the result for r_{max}[30]

$$r_{max} \approx 5.29\ 10^{-9} Z^{-1/3} \text{ cm} \tag{15}$$

Therefore,

$$\log_e \left(\frac{r_{max}}{r_{min}}\right)^{1/2} \approx \log_e 2\,10 Z^{-1/3} \left(\frac{Z}{A}\right)^{1/6} \tag{16}$$

This can be put into a more convenient form by making the approximation

$$\log_e \left(\frac{r_{max}}{r_{min}}\right)^{1/2} \approx \log_e 183 Z^{-1/3} \tag{17}$$

This allows further simplification.[21] Namely, if we measure in

terms of the "radiation length" X_0 defined as

$$\frac{1}{X_0} = \frac{4e^4 NZ}{137 m^2 c^4} (Z + 1) (\log_e 183 Z^{-1/3}) \left[1 + 0.12 \left(\frac{Z}{82}\right)^2\right] \tag{18}$$

$$\langle\theta^2\rangle_{av} \approx \left(\frac{21}{p_{\text{Mev/c}}\beta}\right)^2 X_{\text{rad. length}} \tag{19}$$

where X is measured now in radiation lengths and p is in Mev/c.

Table IV lists radiation lengths for a number of elements. This approach to multiple scattering incorporates the following approximations which have been discussed in detail in the literature:

(1) The assumption that the mean scattering is composed of a very large number of scatterings small compared with the mean leads to the conclusion that over a finite path length the net sum of the deflections has a Gaussian distribution. In fact, this is only partially true and there are a number of scatters greater than the mean deflection. For small deflections the distribution is nearly Gaussian, but for large angles the distribution is very close to that given by the Rutherford formula for single scattering. This results in a "single scattering" tail to the scattering distribution. Figure 4 shows a Gaussian distribution compared with an accurately calculated multiple scattering distribution.[16] For such a distribution it is no longer true that the rms value is the statistically best parameter

Table IV. Radiation Lengths and Critical Energies of Some Typical Substances

Substance	Charge Z	Atomic weight A	Radiation length X_0, g/cm^2	Radiation length, L, cm	Critical energy, Mev: Without density effect	Critical energy, Mev: With density effect
Hydrogen	1	1.01	58	820	340	
He, liquid	2	4	85	680	220	
He, gas (NTP)	2	4	85	4.77×10^5	220	
Carbon	6	12	44.0	19.6	102	76
Water	7.23	14.3	37.1	37.1	83.8	65
Air (NTP)	7.37	14.3	37.1	2.87×10^4	83.8	
Aluminum	13	27	24.5	9.1	48.8	
Iron	26	55.8	14.1	1.83	24.3	21
Copper	29	63.6	13.1	1.52	21.8	
Lead	82	207.2	6.5	0.58	7.8	

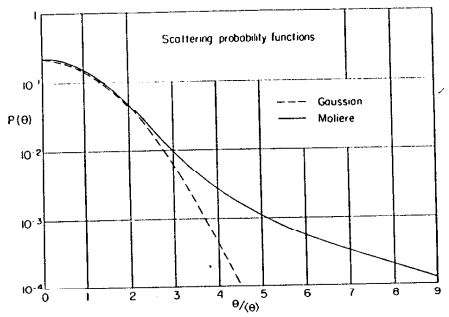

Fig. 4. Comparison of an accurately calculated multiple-scattering distribution of Moliere with that obtained by assuming that the distribution is Gaussian (reference 11).

to measure. The most convenient parameter is the mean value of angles less than 4 times the mean. The theory of such a parameter has been worked out in detail.[16, 29]

(2) In a more complete treatment the detailed problem of which values to choose for θ_{max} and θ_{min} enters. We noted in Section 3 that for small velocities a classical approximation was valid and at large velocities the Born approximation was valid. In the intermediate-velocity region a more sophisticated treatment has been made by Moliere.[16]

(3) In a practical measurement for determining the mean scattering, the net deflection of a particle is measured over some finite length. The track of the particle which is being measured is not perfectly defined in practice and a "sagitta" measurement is usually made on the angle between successive chords. This is easier to measure than a "tangent" and is related to the angle between successive tangents by the factor $(\frac{2}{3})^{1/2}$. The chord lengths are usually chosen such that the "spurious" scattering introduced by the instrument resolution is about $\frac{1}{4}$ of the real multiple scattering.[5]

(4) More information can be obtained by overlapping the measurements. However the additional information is only partially independent and it is not very profitable to take more than one over-lapping set.

(5) The accuracy of a measurement is no longer simply related to the Gaussian analysis. The standard deviation is roughly given by $70\%/\sqrt{n}$, where n is the number of readings.

5. Total Ionization Losses and Probable Ionization Losses

Another useful parameter is the value of the ionization losses as a charged particle traverses a medium. The passage of a charged particle will leave the atoms of the medium excited or ionized and induce the emission of radiation. Various methods of measuring such ionization exist, such as measuring the number of quanta excited in fluorescent substances or the number of grains rendered developable in a nuclear emulsion. These ionization losses can be regarded as due to inelastic Coulomb scattering with electrons as the particle traverses the medium. If the particle has momentum p and suffers a deflection θ in passing an electron, the electron picks up momentum of the order of $p\theta$ and hence energy E_θ of approximately $p^2\theta^2/2m_e$. The number of collisions $I'(\theta)\,d\theta$ with electrons is given by Eq. (10):

$$I'(\theta)\,d\theta = 8\,\frac{\pi N_e z^2 e^4}{(p\beta c)^2}\,x\,\frac{d\theta}{\theta^3} \tag{20}$$

where N_e is the number of electrons per gram. Hence the energy lost per g/cm^2 of path length x is given by

$$-\frac{dE}{dx} = \int_{\theta_{min}}^{\theta_{max}} E_\theta\, I'(\theta)\,d\theta \tag{21}$$

Substituting $I'(\theta)$ from Eq. (20) and putting in the value $E_\theta = p^2\theta^2/2m_e$ gives

$$-\frac{dE}{dx} = 4\,\frac{\pi N_e z^2 e^4}{m_e v^2}\,\log_e\frac{\theta_{max}}{\theta_{min}} \tag{22}$$

Now $p^2\theta^2_{max}/2m_e$ is the maximum transferable energy to an electron, and from kinematics the maximum transferable energy is equal to $(4m_e/M)E$ or $2p^2m_e/M^2$ and thus

$$\frac{p^2\theta^2_{max}}{2m_e} = \frac{2p^2m_e}{M^2} \tag{23}$$

or

$$\theta_{max} = \frac{2m_e}{M} \tag{24}$$

While $\theta_{\min}$ is set by the following condition, if we consider a bound electron with vibrational frequency ν, $h\nu$ being equal to the ionization potential I, a collision to impart energy $h\nu$ must take place in a time T short compared with $1/\nu$. Now T, the collision time, is approximately given by $r/v\gamma$ where r is the impact parameter, v is the velocity, γ is the relativistic factor $1/(1-\beta^2)^{1/2}$, and therefore

$$\frac{r_{\max}}{v\gamma} = \frac{1}{\nu} \quad \text{or} \quad r_{\max} = \frac{v\gamma}{\nu} \tag{25}$$

but from the discussion in Section 3,

$$\theta_{\min} = \frac{\lambda}{r_{\max}} = \frac{h\nu}{pv\gamma} \tag{26}$$

and thus from Eqs. (24) and (26),

$$\frac{\theta_{\max}}{\theta_{\min}} \approx \frac{mv^2\gamma}{h\nu} \tag{27}$$

and hence substituting into Eq. (22)

$$-\frac{dE}{dx} = 4\pi \sum_i \frac{N_{ei} z^2 e^4}{mv^2} \log_e \frac{mv^2\gamma}{h\nu_i} \tag{28}$$

where N_{ei} are number of electrons with ionization potentials i. From the theory of a Thomas-Fermi atom, $\prod_i h\nu_i = (ZI)^Z$, where I is a universal constant.
Therefore,

$$-\frac{dE}{dx} = 4\pi \frac{N_e z^2 e^4}{mv^2} \log_e \frac{mv^2}{ZI(1-\beta^2)^{1/2}} \tag{29}$$

This quantity is known as the total energy loss, and it includes losses from all processes.

If we are interested in losses up to some limiting value $E_{\max}$ this result must be modified. In photographic emulsions, for instance, electrons of energy greater than 5 kv leave the immediate neighborhood of the track and do not contribute to the development of the track. In the emulsion example

$$\frac{p^2\theta^2_{\max}}{2m} \approx E_{\max}, \qquad (E_{\max} \text{ is 5 kv for emulsion}) \tag{30}$$

and, therefore, using the same methods,

$$-\frac{dE_{\text{prob}}}{dx} = 2\pi \frac{N_e z^2 e^4}{mv^2} \log_e \frac{mv^2 E_{\max}}{Z^2 I^2 (1-\beta^2)} \tag{31}$$

The energy-loss formula used can thus always be modified to fit the required physical situation.

It is worth noting that at relativistic velocities the ionization is roughly a function of z^2 and thus, for instance, an α-particle is four times more ionizing than a single charged particle. This property permits charge to be simply determined if it is known that the particle is "relativistic."

6. Range-Energy Curves and Ionization Potentials

The formulas just given are approximate and the accurately derived result for the total energy loss is given by

$$-\frac{dE}{dx} = 4\pi \frac{N_e z^2 e^4}{m_e v^2} \left(\log_e \frac{2m_e v^2}{I\bar{Z}(1-\beta^2)} - \beta^2 \right) - \Sigma_i C_i - \delta \tag{32}$$

where $\Sigma_i C_i$ is the binding-energy term, which is small and results from nonparticipation of tightly bound electrons, and δ is a small correction due to the density of the medium discussed in Section 8. There has been some discussion about the best value of I, the mean ionization potential.[8] The current best value[7] appears to be 12 ev for most elements, except for hydrogen with a value of 18 ev.[27]

Luckily the problem of evaluating range-energy relations is considerably simplified by the fact that once a range-energy relation is known for one particle it can be evaluated for all particles, as is shown below.

The energy loss dE/dx from Eq. (32) is only a function of β for particles of the same charge. Hence

$$\frac{dE}{d\bar{R}} = f_1(\beta) \tag{33}$$

$$\frac{dE/m}{d\bar{R}/m} = f_1(\beta) = f_2(E/m) \tag{34}$$

On integrating,

$$\frac{R}{m} = f_3(E/m) \tag{35}$$

where $f_1(\beta)$, $f_2(\beta_1)$, and $f_3(\beta)$ are functions of β, and the same function is correct for all masses. Thus, if the range-energy curve is known for any particle it can be found for all other particles of the same charge by scaling according to Eq. (35).

This relation is quite generally true and any property such as bubble density in a bubble chamber, which is simply a function of β, will obey a similar law.

The range is a function of the form $E = kR^n$ for low energies, and hence for particles of different mass, the relation is

$$E = km^{1-n}R^n \tag{36}$$

or

$$\frac{p^2}{2m} \propto m^{1-n}R^n \tag{37}$$

and, therefore,

$$R \propto p^{2/n}m^{(n-2)/n} \tag{38}$$

or

$$R \propto m^{2.3}p^{3.3} \tag{39}$$

if $n \leqq 0.6$ (an approximately correct value for nonrelativistic particles). Thus for a group of particles of the same momentum, the range is a strong function of the mass.

In a momentum-analyzed beam, where all the particles have identical momenta, the ranges will simply be proportional to the masses to the $(n-2)/n$ power. Whereas the range-energy relations are sensitive to the exact values of ionization potential, the value of the exponent n is quite insensitive. This has been used as a method to determine mass values of unknown particles.

If an absolute range calibration is required, it is necessary to know the range-energy curve for a given mass value. Table V lists range-energy and energy losses of π's and protons in copper (reference 23 gives complete tables).

7. Delta-Ray Losses

While part of the energy loss of a particle traversing on medium is in the form of excitation and ionization along the track, part of the energy loss is in the form of distinguishable electrons which have resulted from knock on processes. These "knock-on" electrons are known as δ-rays and can be measured and used to provide information similar to that obtained from ionization measurements. From

Table V. Range-Energy and Energy Losses in Copper

E, Mev	R, g/cm²	$-dE/dx$, Mev·cm²/g	E, Mev	R, g/cm²	$-dE/dx$, Mev·cm²/g
		Range of Pions in Copper[a]			
1.202	2.208×10^{-2}	32.81	60.12	1.825×10^{0}	2.081
1.503	3.208	27.80	67.63	2.196	1.975
1.803	4.369	24.24	75.14	2.585	1.891
2.405	7.155	19.48	90.17	3.409	1.768
3.006	1.053×10^{-1}	16.42	105.2	4.282	1.683
3.607	1.447	14.27	120.2	5.192	1.623
4.509	2.139	12.02	135.3	6.132	1.578
5.260	2.804	10.67	150.3	7.095	1.545
6.012	3.546	9.629	180.4	9.071	1.501
6.763	4.364	8.798	225.4	1.211×10^{1}	1.468
7.514	5.254	8.119	300.6	1.727	1.452
9.017	7.244	7.072	375.7	2.244	1.456
10.52	9.500	6.300	450.9	2.758	1.470
12.02	1.201×10^{0}	5.706	526.0	3.266	1.486
13.53	1.476	5.235	601.2	3.769	1.501
15.03	1.775	4.852	676.3	4.266	1.522
18.03	2.438	4.254	751.4	4.757	1.540
22.54	3.584	3.661	901.7	5.722	1.574
30.06	5.852	3.040	1,052.0	6.667	1.605
37.57	8.507	2.659	1,202.0	7.595	1.634
45.09	1.149×10^{1}	2.402	1,353.0	8.507	1.661
52.60	1.475	2.213	1,503.0	9.406	1.685
		Range of Protons in Copper			
1	4.50×10^{-3}	—	250	5.660×10^{1}	2.659
2	1.430×10^{-2}	—	300	7.644	2.402
3	2.840	—	350	9.814	2.213
4	4.666	—	400	1.214×10^{2}	2.081
5	6.848	46.08	450	1.461	1.975
6	9.170	40.46	500	1.720	1.891
8	1.470×10^{-1}	32.81	600	2.268	1.768
10	2.134	27.80	700	2.849	1.683
12	2.907	24.24	800	3.455	1.623
16	4.761	19.48	900	4.080	1.578
20	7.007	16.42	1,000	4.721	1.545
26	1.107×10^{0}	13.42	1,200	6.036	1.501
30	1.423	12.02	1,500	8.056	1.460
35	1.866	10.67	2,000	1.149×10^{3}	1.452
40	2.360	9.629	2,500	1.493	1.456
45	2.901	8.738	3,000	1.835	1.470
50	3.496	8.119	3,500	2.174	1.486
60	4.820	7.072	4,000	2.508	1.501
70	6.321	6.300	4,500	2.838	1.522
80	7.992	5.706	5,000	3.165	1.540
90	9.821	5.235	6,000	3.807	1.574
100	1.181×10^{1}	4.852	7,000	4.436	1.605
120	1.622	4.254	8,000	5.054	1.634
150	2.385	3.661	9,000	5.661	1.661
200	3.894	3.040	10,000	6.258	1.685

[a] From reference 23.

Eq. (20) the probability of a particle of momentum p being deflected by an angle θ is

$$P(\theta)\, d\theta = 8\pi \frac{N_e z^2}{(p\beta c)^2} e^4 x \frac{d\theta}{\theta^3} \tag{40}$$

Noting that the energy E imparted to the electron which caused the deflection is $(p^2\theta^2)/2m_e$, we derive

$$P(E)\, dE = \frac{2\pi N_e z^2 e^4}{mv^2} x \frac{dE}{E^2}$$

or

$$P(E)\, dE = \frac{0.15}{\beta^2} \frac{Z}{A} z^2 x \text{ g/cm}^2 \frac{dE_{\text{Mev}}}{E^2_{\text{Mev}}} \tag{41}$$

or, more conveniently,

$$P(E)\, dE = W \frac{dE}{E^2}$$

where

$$W = \frac{0.15}{\beta^2} \frac{Z}{A} z^2 x \text{ Mev} \tag{42}$$

Thus the number of δ-rays with energies greater than E in an average track is just W/E. If, for example, a track with $\beta = 1$ traverses 1 g/cm^2 of material with $Z/A = \frac{1}{2}$, we will find five δ-rays whose energies exceed 15 kv, W being equal to 75 kv.

For a relativistic track $\beta = 1$, the δ-ray density is just a function of z^2 where z is the charge of the incident particle.

8. Ionization Plateau and Density Effect

The initial behavior of the ionization given by Eq. (31) is that it starts decreasing proportional to β^{-2}, and then the logarithmic term containing the factor $1/(1 - \beta^2)$ causes a slow increase in the relativistic region.

However, as was pointed out by Fermi,[9] this increase does not continue indefinitely, as the derivation does not take into account the shielding of the field at large distances due to the macroscopic dielectric properties of the medium. The macroscopic dielectric properties reduce the field at large impact parameters.

The solution of the problem can be easily approximated, as shown by Bohr,[4] by considering that this screening becomes effective at impact parameters of

$$r_{\max} \approx \left(\frac{mc^2}{4\pi N_e e^2}\right)^{1/2}, \qquad (N_e = \text{electron density})$$

Below this impact parameter the usual formula is correct; at distances greater than this impact parameter, no energy transfers occur, owing to dielectric shielding. Substituting this value into the derivation in Section 5 for the probable energy losses, we obtain in the limit $\beta = 1$

$$\frac{dE}{dX} = 2\pi \frac{Nz^2e^4}{mc^2} \left(\log_e \frac{m^2c^2E_{\max}}{4\pi N_e e^2 \hbar^2} - 1\right) \tag{43}$$

The behavior of the ionization is that it drops initially, almost as the inverse square of the velocity, reaches a minimum value called the "minimum ionization," and starts rising as the maximum effective impact parameter increases, until it reaches the plateau value given above. It has been suggested that this increase could be used as the basis of relativistic energy measurements. This relativistic rise varies from about 10 percent in condensed media to about 60 precent in dilute gases (Fig. 5)

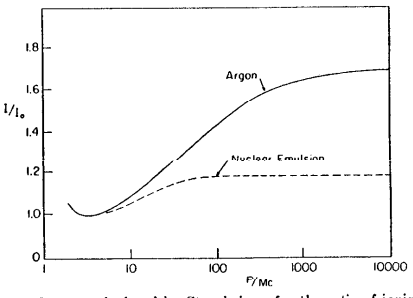

Fig. 5. Curves calculated by Sternheimer for the ratio of ionization to minimum ionization for argon at atmospheric pressure, and photographic emulsion as a function of the momentum in units of the rest mass.

These results have been refined and worked out in great detail by various authors[27] and have been experimentally verified.

9. Collision Processes and the "Geometric Cross Section"

All the "strongly interacting" particles, which includes all particles except the μ-meson, electron, and neutrino, will collide inelastically with nuclei, thus leading to scattering or absorption in the nuclei.

For most purposes in the design of experiments, this inelastic cross section can be approximated by regarding the nucleus of atomic weight as an opaque sphere of radius R, given by

$$R = 1.1 \times 10^{-13} A^{1/3} \tag{44}$$

Thus the cross-sectional area presented by one nucleus is

$$\sigma = \pi R^2 = 4 \times 10^{-26} A^{2/3} \text{cm}^2 \tag{45}$$

The mean force path λ in g/cm^2 for a collision in nuclear matter is then given by

$$\lambda = \frac{1}{N\sigma} \tag{46}$$

where N is the number of nuclei per gram and, therefore,

$$\lambda = 43.7 A^{1/3} \text{ g/cm}^2 \tag{47}$$

where σ and λ are called, respectively, "geometrical cross sections" and "geometrical mean free paths." Naturally current values should be looked up from a given particle or energy if more than the order of magnitude is required. However, for example, a beam of π-mesons in carbon with ranges greater than the mean free path of $\sim$100 g/cm^2 will generally be attenuated by collisions and not by ionization losses. Thus ionization ranges for π-mesons above 150 Mev become increasingly hard to measure.

10. Fluctuations in Ionization Losses

A very important consideration in the design of an experiment is the theoretical precision attainable in the measurement of ionization values.

There are two possible cases, as will be shown. In the first case a large number of collisions involving maximum energy transfer occur during a traversal, and, as the total energy transfer is made up of a multitude of small energy losses, the fluctuations are Gaussian. For

nonrelativistic particles losing a reasonable fraction of their energy ($\sim$10 per cent) this case is applicable, and the theoretically attainable precision goes inversely as the square root of the energy loss. These conditions occur for solid scintillators and Cerenkov counters.

However, when the maximum transferable energy has a very low probability of occurring in one traversal, doubling the energy loss in the detector merely doubles the probability of obtaining a large fluctuation, and the theoretically attainable precision becomes almost independent of the thickness. This latter case has been considered in detail by Landau[15] and Symons.[26] This case is applicable to relativistic particles under most conditions and to nonrelativistic particles traversing thin counters (i.e., gas counters of all types; cf. Chapter VI).

We shall now outline a simple treatment that gives the respective conditions of applicability for these two cases.

As has been shown in the previous section, the formula for the distribution of energy losses in a path of x g/cm^2 is given by Eq. (42).

$$P(E)\, dE = W(dE/E^2)$$

where

$$W_{\text{Mev}} = \frac{0.15\, Zx}{\beta^2\, A} \tag{48}$$

The probability $P(>E)$ for a collision of energy greater than E to occur is given by

$$P(>E) = \int_E^\infty \frac{W\, dE}{E^2} = W/E \tag{49}$$

The condition for there to be a number of transfers of energy near $E_{\max}$ is therefore given by

$$P(>E_{\max}) \gg 1 \tag{50}$$

or by

$$W/E_{\max} \gg 1$$

This case will be treated first and corresponds to the Gaussian fluctuation. For

$$W/E_{\max} \ll 1 \tag{51}$$

the Landau approximation will be valid and the fluctuations become almost independent of the thickness.

The maximum possible energy given an electron $E_{\max}$ is given by $(4m/M)E$ in the nonrelativistic case and by $\sim[(E/Mc^2)^2]2m_ec^2$ in the relativistic region, the general formula being

$$E_{\max} = 2\,\frac{(E + Mc^2 + m_ec^2)^2 m_e c^2}{M^2c^4 + m_e^2c^4 + 2m_ec^2(E + Mc^2)} - 2m_ec^2$$

or

$$E_{\max} \approx \frac{2\beta^2}{1-\beta^2}\, m_e c^2 \tag{52}$$

By putting $Z/A \approx \frac{1}{2}$ and using Eq. (50), the condition for the Gaussian distribution to be valid is

$$\beta^4/1 - \beta^2 \ll 0.074x \tag{53}$$

and for the Landau distribution to hold,

$$\beta^4/1 - \beta^2 \gg 0.074x \tag{54}$$

Thus a nonrelativistic proton $\beta \sim \frac{1}{3}$ (energy ~ 50 Mev) traversing a 1-g scintillation crystal will meet condition (53) and thus give Gaussian fluctuations; for $\beta^4/1 - \beta^2 \sim \frac{1}{80}$. On the other hand, a 1-Bev μ-meson traversing a 10-g scintillation crystal will have $\beta^4/1-\beta^2 \sim 100$ and will meet condition (54) for Landau fluctuations.

It can be seen that the $\beta^4/(1 - \beta^2)$ functional dependence means that there is a fairly sharp transition from the region of validity of one approximation to that of the other approximation. Thus most physical situations can be described by one or the other formula.

10.1. *Gaussian Fluctuations in Ionization Losses*

We have seen from Eqs. (43) and (44) that the energy loss W is a convenient parameter to determine whether to use the Gaussian or Landau fluctuation formulas. In terms of W the energy-loss formula is

$$P(E)\,dE = W(dE/E^2) \tag{55}$$

and the average energy loss, if W is very much greater than $E_{\max}$, is given as

$$\langle E\rangle_{\text{av}} = \int_{E_{\min}}^{E_{\max}} EW\,\frac{dE}{E^2} = W \log_e \frac{E_{\max}}{E_{\min}} \tag{56}$$

The rms fluctuation is

$$\langle (E - \langle E\rangle)^2\rangle^{1/2} \approx W^{1/2}E_{\max}^{1/2} \tag{57}$$

and thus the fractional rms deviation σ in the energy loss is given by

$$\sigma = \frac{\langle (E - \langle E\rangle_{\text{av}})^2\rangle^{1/2}}{\langle E\rangle_{\text{av}}} = \frac{W^{1/2}E_{\max}^{1/2}}{W \log_e (E_{\max}/E_{\min})} \tag{58}$$

This can be rewritten as

$$\sigma^2 = \frac{E_{\max}/\log_e (E_{\max}/E_{\min})}{W \log_e (E_{\max}/E_{\min})} = \frac{E_{\max}/\log_e (E_{\max}/E_{\min})}{E_{\text{av}}} \tag{59}$$

by using Eq. (56), or as

$$\sigma = E_{\text{eff}}^{1/2}/E_{\text{av}}^{1/2} \tag{60}$$

where

$$E_{\text{eff}} = \frac{E_{\max}}{\log_e (E_{\max}/E_{\min})} \tag{61}$$

If the effective number of collisions N is defined as $N = E_{\text{av}}/E_{\text{eff}}$,

$$\sigma = 1/N^{1/2} \tag{62}$$

Thus we obtain a simple model which gives the correct results. We simply regard all losses as occurring with

$$E_{\text{eff}} = \frac{E_{\max}}{\log_e (E_{\max}/E_{\min})}$$

and then the fluctuation goes inversely as the square root of the number of collisions.

From Section 5,

$$\log_e \frac{E_{\max}}{E_{\min}} = \log_e \frac{m_e^2v^4}{Z^2I^2(1-\beta^2)} \tag{63}$$

This is a slowly varying function and is approximately equal for $Z = 26$ and $\beta = \frac{1}{3}$ to 15. Thus $E_{\text{eff}} \approx E_{\max}/15$.

By applying these considerations for instance to a 50 Mev proton traversing a 1-g/cm^2-thick scintillator, the maximum kinetic energy is $E_{\max} = 4m/M \times 50$ Mev ≈ 110 *kv*. The effective energy loss is $\frac{1}{15}$ of this, or 7 kv; the parameter W is 675 kv, from Eq.

(48); and the average energy lost per gram is 15×675 kv, or 10 Mev, from Eq. (56). The average energy loss of 10 Mev divided by the effective energy loss of 7 kv gives an effective number of 1,400 collisions or a percentage theoretical rms error of $1/(1{,}400)^{1/2} \sim 3$ percent, for the fluctuation in energy losses.

The effective energy loss is a particularly useful concept for rule-of-thumb calculations. Thus, as will be discussed in the chapter on scintillation crystals, an energy loss of about 4 kv is required to release a photoelectron from the photomultiplier surface, and thus in the example above the statistical fluctuations in the number of photoelectrons released will be less important than the intrinsic energy fluctuations. It can readily be seen that there will be cases for which the major fluctuations are contained in the measuring equipment, and other cases for which the maximum attainable theoretical precision will be the limitation. In the case outlined above there would be no significant increase in precision in setting up systems for which more than one photoelectron was released per 3 kv energy loss.

10.2. *Landau Fluctuations in Ionization Losses*

For $W \ll E_{\max}$, i.e., for the case in which maximum energy loss occurs with small probability for one traversal, the probable energy loss becomes

$$\langle E \rangle \approx \int_{E_{\min}}^{4W} EW \frac{dE}{E^2} \tag{64}$$

$$= W \log_e (4W/E_{\min}) \tag{65}$$

and the rms fluctuation, ignoring improbable collisions, is

$$\sigma^2 = \frac{\langle (E - \langle E \rangle_{\text{av}})^2 \rangle}{\langle E \rangle_{\text{av}}^2} \approx \int_{E_{\min}}^{4W} E^2 W \frac{dE/E^2}{\langle E \rangle_{\text{av}}^2} \tag{66}$$

and, therefore,

$$\sigma \approx 2W/E_{\text{av}} \tag{67}$$

Thus combining (65) and (66)

$$\sigma \approx \frac{2}{\log_e (W/E_{\min})} \tag{68}$$

This result is almost independent of the material or thickness.

Another way of expressing the result given by Eq. (66) is that $\langle (E - \langle E \rangle_{\text{av}})^2 \approx 4W^2$, or that the rms fluctuation in energy is measured, for all cases for which the Landau fluctuation applies, in units of W.

Landau has carried through the calculation precisely and obtains the curves given in Fig. 6 for the integral and differential probability distributions for the occurrence of fluctuations about the mean energy measured in units of W.

As W is approximately $\frac{1}{20}$ of the average energy loss, the ordinates multiplied by 5 will give approximately the percentage energy deviation from the mean (Fig. 6).

11. Fluctuations in Range

Particles other than electrons which lose energy in radiation processes (Section 14), will have a range straggling[25] which can be simply evaluated:

$$\langle (R - \langle R \rangle_{\text{av}})^2 \rangle_{\text{av}}^{1/2} = \left(\frac{200 m_e}{M}\right)^{\frac{1}{2}} f\left(\frac{E}{Mc^2}\right) \tag{69}$$

where R is the range and M the mass of the particle and E its energy.

Figure 7 shows the function $f(E/Mc^2)$ as a function E/mc^2.

For example, for a μ-meson whose mass is 200 m_e and whose kinetic energy equals its rest mass (100 Mev), the rms straggling error in range from Fig. 7 is 2.8 percent.

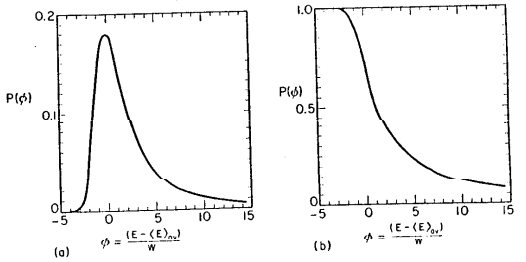

Fig. 6. (a) The differential probability for a given fluctuation of energy, in units of W, Eq. (48). (b) The integral probability of finding a fluctuation greater than a given value, in units of W.

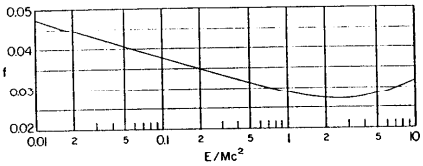

Fig. 7. The fraction $f(E/Mc^2)$ that is used in formula (69) to describe the rms fluctuation in range as a function of the kinetic energy measured in units of rest mass.

12. Kinematic Considerations on Decay Processes

Many experiments make use of the constraints provided by kinematic considerations to provide information. The uses divide into three main categories. First, in the collision of particles (sometimes uncharged) with a proton, the recoiling proton provides data on the incident particle. Second, the "threshold" energies for the occurrence of certain reactions can be used to ensure that these reactions are in fact those being recorded by the experimental apparatus. Third, in decay or production processes, angular and energy correlations occur which provide signatures for events. Such signatures for instance are the decay of, $\pi^\circ \rightarrow 2\gamma$, or $\Lambda^\circ \rightarrow \pi^- + P$.

In analyzing relativistive kinematics, a convenient device is to evaluate problems in the "center-of-mass frame" in which the net momentum of the total system is zero. The reasons for this are three-fold. First, the minimum energy for a production process to occur is when the products in the center-of-mass system are produced with no net kinetic energy or "at rest." Second, the center-of mass system automatically displays the symmetries of the problem. For instance, when a proton strikes another proton in the center-of-mass system, the protons are moving toward each other with identical velocities and are thus on an identical footing. Finally the formulas are mathematically simplest in this system.

The necessary relativistic formulas and transformations can be found in standard texts and are listed without derivation.

The total energy E is given as

$$E = \frac{m_0c^2}{(1-\beta^2)^{1/2}} \quad \text{or} \quad E = \gamma m_0 c^2 \tag{70}$$

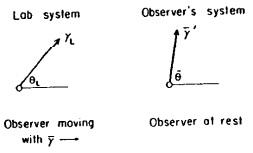

Fig. 8

where

$$\gamma = \frac{1}{(1-\beta)^{1/2}} \tag{71}$$

The momentum is given by

$$p = \frac{m_0c\beta}{(1-\beta^2)^{1/2}} \quad \text{or} \quad p = \gamma\beta m_0 c \tag{72}$$

Where m_0 is the rest mass and β the ratio of the velocity to the velocity of light.

Derived from these we have

$$E^2 = p^2c + m_0{}^2c^4 \tag{73}$$

To transform a particle with γ_L into the coordinate frame of an observer moving with $\bar{\gamma}$ and at an angle θ to the motion of the particle so that in the frame of the observer it will move with $\bar{\gamma}^1$ and at an angle $\bar{\theta}$, we note the following relations (Fig. 8):

$$\gamma_L = \bar{\gamma}'\bar{\gamma} + \sqrt{(\bar{\gamma}^2 - 1)}\sqrt{(\bar{\gamma}'^2 - 1)}\cos\bar{\theta} \tag{74}$$

and

$$\bar{\gamma}' = \gamma_L\bar{\gamma} - \sqrt{(\bar{\gamma}^2 - 1)}\sqrt{(\gamma_L{}^2 - 1)}\cos\theta_L \tag{75}$$

For a light quantum of frequency ν the relations above are replaced by

$$E = h\nu \tag{76}$$

$$p = \frac{h\nu}{c} \tag{77}$$

and the transformation to the frame of an observer moving with $\bar{\gamma}$ at an angle θ_L (Fig. 9) leads to

$$\nu_L = \bar{\nu}(\bar{\gamma} + \sqrt{(\bar{\gamma}^2 \quad 1)}\cos\bar{\theta}) \tag{78}$$

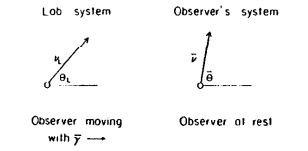

Fig. 9

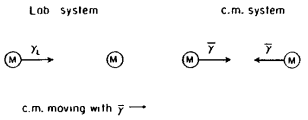

Fig. 10. The lab and center-of-mass systems for the collision of two identical particles.

or

$$\nu_L = \bar{\nu}(1 + \bar{\beta}\cos\bar{\theta})/(1 - \bar{\beta}^2)^{1/2} \tag{79}$$

also

$$\bar{\nu} = \nu_L(\bar{\gamma} - \sqrt{(\bar{\gamma}^2 - 1)}\cos\theta_L) = \nu\frac{1 - \bar{\beta}\cos\theta_L}{(1 - \bar{\beta}^2)^{1/2}} \tag{80}$$

where $\bar{\nu}$ is the frequency in the observer's system and $\bar{\theta}$ the angle.

12.1 *Kinematics of the Collision of Two Particles of Identical Mass, One of which is at Rest*

Figure 10 shows the lab and center of mass system for the collision of two identical particles. To determine the $\bar{\gamma}$ of the center-of-mass system we proceed as follows using formula (75) to connect the two systems, observing that in formula (75) $\bar{\gamma}' = \bar{\gamma}$ and that as the collision is head on, $\theta_L = \bar{\theta} = 0$. We find

$$\gamma_L = 2\bar{\gamma}^2 - 1 \tag{81}$$

Thus we determine the value of $\bar{\gamma}$ for the center-of-mass system in terms of γ_L.

An alternative derivation is to note that the total energy in the center-of-mass system is $2\bar{\gamma}Mc^2$. The total momentum is zero.

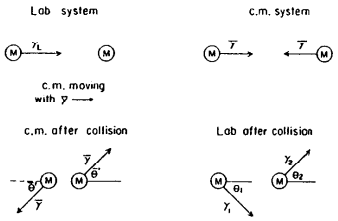

Fig. 11

Thus the system is equivalent to a particle of mass $2\bar{\gamma}M$ at rest, and, in fact, the two incident particles could, while conserving energy and momentum, fuse to form such a particle. Such a particle at rest transformed into a system moving with $\bar{\gamma}$ would have a total lab energy of $\bar{\gamma}$ times its mass, or

$$E_L = 2\bar{\gamma}^2Mc^2 \tag{82}$$

However, we already know the lab energy E_L is

$$E_L = \gamma_L Mc^2 + Mc^2 \tag{83}$$

Thus again we find by combining Eqs. (82) and (83) that

$$\gamma_L = 2\bar{\gamma}^2 - 1 \tag{84}$$

Knowing $\bar{\gamma}$ we can evaluate the transformations and kinematics of elastic collision processes. In an elastic collision process energy and momentum are conserved and thus the particles rebound in the center-of-mass system with only a change of direction (Fig. 11).

The only arbitrary parameter is $\bar{\theta}'$, the scattered angle in the center-of-mass system; the other parameters are directly derivable from Eqs. (74) and (84) in terms of $\bar{\theta}'$.

12.2. *Kinematics of the Collision of Two Particles of Different Masses*

Figure 12 shows the lab and center-of-mass system for two particles colliding with different masses. The center of mass $\bar{\gamma}$ can be determined by noting that the total center-of-mass energy $E_{c.m.}$ is given by

$$E_{c.m.} = M_1c^2\bar{\gamma}_1 + M_2c^2\bar{\gamma} \tag{85}$$

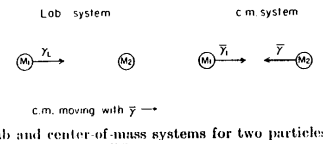

Fig. 12. The lab and center-of-mass systems for two particles colliding with different masses.

The net momentum is zero in the center-of-mass system and, therefore, using the relativistic formula for momentum [Eq. (72)]

$$M_1\sqrt{(\bar{\gamma}_1^2 - 1)} - M_2\sqrt{(\bar{\gamma}^2 - 1)} = 0 \tag{86}$$

and, therefore,

$$M_1\bar{\gamma}_1 = (M_2^2\bar{\gamma}^2 - M_2^2 + M_1^2)^{1/2} \tag{87}$$

Substituting Eq. (87) into Eq. (85) gives

$$E_{\text{c.m.}} = c^2(M_2^2\bar{\gamma}^2 - M_2^2 + M_1^2)^{1/2} + M_2c^2\bar{\gamma} \tag{88}$$

Now

$$E_{\text{lab}} = \bar{\gamma}\, E_{\text{c.m.}} \qquad \text{[c.f. Eq. (82)]} \tag{89}$$

and thus combining Eqs. (88) and (89),

$$E_{\text{lab}} - M_2c^2\bar{\gamma}^2 = \bar{\gamma}c^2\,(M_2^2\bar{\gamma}^2 - M_2^2 + M_1^2)^{1/2} \tag{90}$$

Squaring and rearranging,

$$\bar{\gamma} = \frac{E_{\text{lab}}}{(M_1^2c^4 - M_2^2c^4 + 2M_2c^2E_L)^{1/2}} \tag{91}$$

but from Eq. (89),

$$E_{\text{c.m.}} = \frac{E_{\text{lab}}}{\bar{\gamma}} \tag{92}$$

and, therefore,

$$E_{\text{c.m.}} = (M_1^2c^4 - M_2^2c^4 + 2M_2c^2E_L)^{1/2}$$

which for $M_1 = M_2$ is equivalent to Eq. (82).

In a pion-proton collision in which the pion is absorbed, the maximum energy available for forming other products is

$$(M_\pi^2c^4 + M_p^2c^4 + 2M_pc^2E_\pi)^{1/2} - M_pc^2$$

corresponding to the proton being left at rest after the collision.

For a γ-ray collision with a proton, the maximum possible energy available is

$$(M_p^2c^4 + 2E_\gamma M_pc^2)^{1/2} - M_pc^2 \tag{94}$$

This can be readily seen as the limit for $M_1 \to 0$.

This threshold energy represents a very valuable check in many experiments. For instance if the process $\gamma + p \to \pi^\circ + p$ is being studied, we know that π° production is impossible for energies smaller than 145 Mev, and increases sharply for higher energies.

Another use of the kinematic relationships is in an elastic scattering reaction of particles of unequal masses, such as $K^+ + P \to K^+ + p$. The method of evaluation is shown diagrammatically in Fig. 13 using the $\bar{\gamma}$ given by Eq. (81). The angles and energies necessary to conserve momentum and energy are characteristic of this process and can be distinguished from elastic proton or pion-proton collisions. Kinematic relations can also distinguish the reactions of π^- on a free proton in a propane bubble chamber from π^- on the carbon in the chamber.

$$\pi^- + P \to \Lambda^\circ + \theta^\circ$$

In this reaction, if the π^- energy is known, the angles that Λ and θ° make to the direction of the π^- are uniquely related. If the

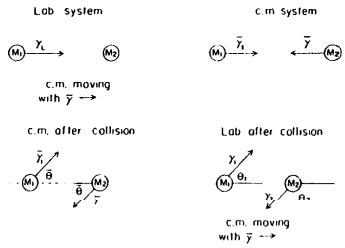

Fig. 13

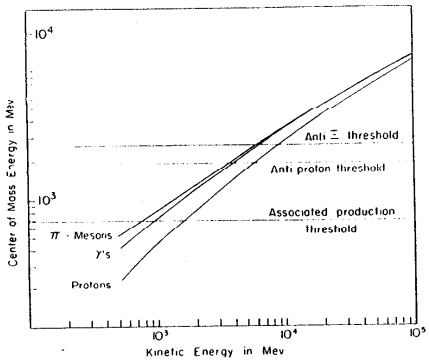

Fig. 14. Center-of-mass energies for incident primary energies of γ-rays, π-mesons, and protons.

one angle is known then all the rest of the angles and energies can be deduced and compared with observation. A diagram such as Fig. 13 combined with Eq. (91) will give the resultant kinematics.

Figure 14 shows center-of-mass energies for incident primary energies of γ-rays, π-mesons, and protons.

12.3. *Kinematic Correction for the Effect of Fermi Momentum in Collisions with Nuclei*

A large fraction of high-energy physics is concerned not with interactions with single particles but with collision processes with complex nuclei. Two procedures suggest themselves in analyzing such situations. The first is to use the formulas previously derived and substitute the atomic weight A for the mass of the struck particle. This is satisfactory only for the very rare case in which the nucleus is left unperturbed after the collision. The DeBroglie wavelength of the incident particle, however, is usually very small compared with the size of the nucleus and thus the interaction is only with a small fraction of the nucleus. The second procedure is to make the approximation that the incident particle sees only one nucleon as it interacts and to use the formulas derived from collisions with free protons.

This is more satisfactory, but in practice a closer approximation is to consider that the nucleons in a complex nucleus move with a distribution of momenta ("Fermi momenta"). The collisions then are not with particles at rest, but with moving particles.

The procedures outlined in the preceding sections are perfectly adequate, albeit tedious, to solve the kinematics. To ensure that the results make physical sense, however, the momentum of the struck nucleon after the collision has to belong to a physically possible excited state and not to a state forbidden by the Pauli exclusion principle. As an example we work out the change in center-of-mass energy resulting from the Fermi momenta (Fig. 15).

If the lab system in which a particle of mass M_p is approaching a moving nucleon is transformed to the "pseudo-lab (dashed) system" where the nucleon is at rest, the ratio

$$\frac{\gamma_L' - \gamma_L}{\gamma_L} \tag{95}$$

represents the fractional apparent gain in lab energy.

Now

$$\gamma_L' = \gamma_L\gamma_F + \sqrt{(\gamma_L^2 - 1)}\sqrt{(\gamma_F^2 - 1)}\cos\theta \tag{96}$$

If γ_L' and γ_L are large and the struck nucleon is nonrelativistic (which is always true in practice),

$$\sqrt{(\gamma_L^2 - 1)} \approx \gamma_L \tag{97}$$

and

$$\gamma_F \approx \left(1 + \frac{P_F^2}{2M_p^2}\right) \approx 1 \tag{98}$$

From Eq. (73),

$$\sqrt{(\gamma_F^2 - 1)} = \frac{P_F}{M_pc} \tag{99}$$

Then substituting these values in Eq. (96),

$$\gamma_L' \approx \gamma_L + \gamma_L \frac{P_F \cos\theta}{M_pc} \tag{100}$$

and

$$\frac{\gamma_L' - \gamma_L}{\gamma_L} = P_F \frac{\cos\theta}{Mc} \tag{101}$$

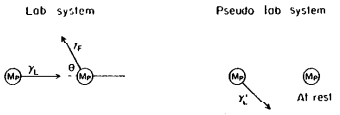

Fig. 15. The change in center-of-mass energy resulting from the Fermi momenta.

In practice $P_F/Mc \approx \frac{1}{5}$ at its maximum value, and the effective center-of-mass energy for a collision on a nucleus is thus increased by 20 percent. For example, a 6-Bev proton incident on a nucleus can have an equivalent center-of-mass energy to a 7.2-Bev proton incident on a free proton.

13. Kinematic Correlations in Decay Processes

In many experiments it is not necessary to measure all properties of the system. A few well-chosen measurements combined with kinematic theory enable the correct conclusions to be drawn. For instance in the decay process $\pi^\circ \rightarrow 2\gamma$, the angle between the two γ-rays bears a relation to the π°-energy and it is not necessary for a number of applications to do anything but measure this angle to estimate the direction and energy of the π°-meson.

Similarly, in observations on relativistic decays of θ°-mesons $\rightarrow \pi^+ + \pi^-$ and $\Lambda^\circ \rightarrow p + \pi^-$, where due to the relativistic nature of the tracks only the momenta and sign of the particles are known (not the identity), it is still possible to measure the fraction of decays due to Λ's and θ's as explained in Section 13.2.

The examples given below are for the purpose of illustrating how general properties may be extracted.

13.1. *General Result on the Energy of the Products of Two-Body Decay*

If a process such as

$$\pi^- + p \rightarrow \pi^\circ + N$$
$$\downarrow$$
$$2\gamma$$

is investigated in order to determine the energy of the π° and hence the Q of the reaction, it might at first sight be thought that both γ-rays from the π° would have to be simultaneously measured.

However, a measurement of the energies of one of the γ-rays is sufficient if it is assumed that the decay is isotropic.

This follows because, as will be proved, the energy distribution of the γ-rays is uniform between two extreme values, twice the geometric mean of the maximum and minimum γ-ray energies gives the π°-mass value, and the breadth of the distribution gives the π°-velocity.

Consider a two-body decay in the center-of-mass and lab systems (Fig. 16).

Then from Eq. (74),

$$\gamma_1 = \bar{\gamma}\bar{\gamma}_1 + (\bar{\gamma}^2 - 1)^{1/2}(\bar{\gamma}_1^2 - 1)^{1/2}\cos\bar{\theta} \qquad (102)$$

However, if the decay is isotropic in the center-of-mass system so that the number of decays into unit solid angle is constant, then the number of decays is proportional to $d\Omega$ ($d\Omega$ is the solid angle) or to $d\cos\bar{\theta}$. However the lab energy is of the form $a + b\cos\bar{\theta}$ [Eq. (102)] and hence the energy spectrum is uniform from $a + b$ to $a - b$, the maximum and minimum energies, respectively.

Alvarez et al.[1] use this property. In the capture of K^--mesons at rest,

(a) $$K^- + P \rightarrow \Lambda^\circ + \pi^\circ$$

and

(b) $$K^- + P \rightarrow \Sigma^\circ + \pi^\circ \rightarrow \Lambda^\circ + \gamma + \pi^\circ$$

The Λ°'s from process (a) are more energetic whereas the Λ°'s from process (b) have a distribution spread in energy in the form of a

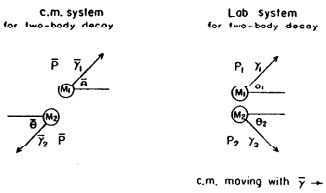

Fig. 16. A two body decay in the center-of-mass and lab systems.

square pulse as shown above. This permits channels (a) and (b) to be distinguished quantitatively by observing the Λ^0-spectrum.

A second general property follows from Eq. (102). Putting $\cos\theta = +1$ and -1,

$$(E_{\max}E_{\min})^{1/2} = M_1c^2(\bar{\gamma}^2 + \bar{\gamma}_1^2 - 1)^{1/2} \tag{103}$$

For a π^0-decay into two γ-rays, $\pi^0 \rightarrow \gamma + \gamma$, we find in a similar way,

$$(E_{\max}E_{\min})^{1/2} = h\bar{\nu}_\gamma = \tfrac{1}{2}M_{\pi^0}c^2 \tag{104}$$

The breadth of the γ-ray energy distribution $E_{\max} - E_{\min}$ is simply $2(\bar{\gamma}^2 - 1)M_{\pi^0}c^2$, thus allowing the $\bar{\gamma}$ of the π^0 and hence its velocity to be measured.

Thus by measuring the spectrum of single γ-rays arising from the process

$$\begin{array}{c} \pi^- + P \rightarrow \pi^0 + N \\ \downarrow \\ 2\gamma \end{array}$$

Panofsky et al.[20] were able to measure the velocity of the π^0's, and, knowing the proton and neutron mass difference, they then calculated the $\pi^- - \pi^0$ mass difference.

Another feature of two-body decays is the angle between the decay products. While the distributions are complicated, a quick guide can be obtained as the maximum available solid angle in the center-of-mass system is at 90 degrees and hence the typical decay occurs at an angle around 90 degrees. A property of relativistic transformations is that transverse momenta are unchanged (Fig. 17). Hence the typical laboratory angle is given as

$$\sin\theta = \frac{P_T}{P_L} = \frac{\bar{\gamma}_1^2 - 1}{\bar{\gamma}_1^2\bar{\gamma}^2 - 1} \tag{105}$$

and for large $\bar{\gamma}$ of the center-of-mass system this reduces to

$$\sin\theta \sim \frac{1}{\bar{\gamma}} \tag{106}$$

Many studies of π^0-production have been made in which the apparatus has consisted of two telescopes designed to pick up both

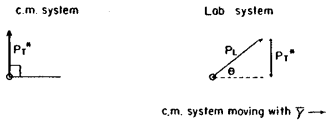

Fig. 17

γ-rays from the π-decay with a given angular separation. At any given angle the telescope is largely recording π^0's in a specific energy band.[25]

This property applies also to nuclear interactions in which the center-of-mass system $\bar{\gamma}$ determines the half-width of the angular distribution of products as approximately $1/\bar{\gamma}$ radian.

13.2. *Manchester α-Parameter for Identifying Neutral Decays*

Another very useful correlation exists which has been used to characterize relativistic decays in flight of neutral particles.

If we consider a two-body neutral decay into two identical particles, the two particles will tend to go off with equal momenta. This is because the amount of solid angle available in the center-of-mass system is greatest at 90 degrees, and thus on the average the decay products will be emitted symmetrically.

If, however, the decay products are very dissimilar in mass, their momenta in the lab system will be approximately proportional to their masses and hence very dissimilar. As the transverse momenta are equal, this is equivalent to saying that the angles of emission will be inversely proportional to the masses. The quantitative parameter α chosen to measure this simple property is:[3,28]

$$\alpha = \frac{p_1^2 - p_2^2}{P^2} = \frac{\sin^2\theta_1 - \sin^2\theta_2}{\sin^2(\theta_1 + \theta_2)} \approx \frac{\theta_2 - \theta_1}{\theta_2 + \theta_1} \tag{107}$$

where p_1 is the momenta of the first particle, p_2 of the second particle, and P the total momenta; θ_1 is the direction particle one makes with the line of flight and θ_2 is the direction particle two makes with the line of flight (see Fig. 16).

If the particles in the lab are highly relativistic and not relativistic in the center-of-mass system, then the following are satisfac-

tory approximations:

$$\begin{aligned} l' &= \bar{\gamma}(M_1c + M_2c) \\ p_1 &\approx \gamma_1 M_1 c \\ p_2 &\approx \gamma_2 M_2 c \end{aligned} \tag{108}$$

By the use of the approximations of Eq. (108) and substituting into eq. (107),

$$\alpha \approx \frac{M_1\gamma_1^2 - M_2\gamma_2^2}{(M_1 + M_2)\bar{\gamma}^2} \tag{109}$$

and noting $\bar{p}_1 = \bar{p}_2 = \bar{p}$ where $\bar{p}$ is the momentum in the center-of-mass system of the two decay products,

$$\alpha \approx M_1^2 \frac{[\bar{\gamma} + (\bar{p}\bar{\gamma} \cos \bar{\theta}/M_1c)]^2 - M_2^2[\bar{\gamma} - (\bar{p}\bar{\gamma} \cos \bar{\theta}/M_1c)]^2}{(M_1 + M_2)^2\bar{\gamma}^2} \tag{110}$$

$$\alpha \approx \frac{M_1 - M_2}{M_1 + M_2} + \frac{2\bar{p} \cos \bar{\theta}}{(M_1 + M_2)c} \tag{111}$$

It is again true as in the previous section that for an isotropic decay the α-value distribution will be a "square" pulse with an average value $(M_1 - M_2)/(M_1 + M_2)$.

Thus if we have no other information than momentum measurements or angles available, it is still possible to differentiate between two different decay possibilities such as

$$\Lambda_0 \rightarrow l' + \pi^- \qquad \text{or} \qquad \theta^0 \rightarrow \pi^+ + \pi^-$$

It is unusually possible to determine if the decay is a decay into two bodies by a coplanarity test (conservation of momentum).

14. Electromagnetic Interactions

14.1. *Electrons and γ-Rays*

Electrons and γ-radiation have "electromagnetic" properties which permit easy identification and separation. Owing to their small masses, electrons readily accelerate or decelerate in collision processes and thus radiate electromagnetic radiation. The reverse process in which γ-radiation interacts with electrons has a large cross section, and this permits unequivocal differentiation of γ-rays from other neutral particles.

Electromagnetic processes have another feature. As discussed in Section 13, nuclear interactions are characterized by the products being emitted into angles of the order of $1/\bar{\gamma}$ or $(2M_\mu c^2/W)^{1/2}$. Thus for instance in a 5-Bev proton-proton collision the products are spread over a 20-degree opening angle.

However, for electromagnetic processes the typical angle is of the order of $m_e c^2/E$. A 5-Bev electron radiating a γ-ray will radiate into an opening angle of 0.05 degree. This results from the fact that electromagnetic collisions generally involve small traverse momentum transfers of the order of $m_e c$ or less.

Electromagnetic cross sections and mean free paths are usually calculated in terms of a natural unit called the radiation length, i.e., the length required on the average for a high-energy electron to degrade its energy to $1/e$ of its initial value. In terms of this unit all substances have nearly identical cross sections.

The radiation length X in g/cm^2 is defined as

$$\frac{1}{X} = N \frac{4Z(Z + 1)}{137} \left(\frac{e^2}{m_e c^2}\right)^2 (\log_e 183\, Z^{-1/3}) \times \left[1 + 0.12\left(\frac{Z}{82}\right)^2\right] \tag{112}$$

N being the number of atoms per g/cm^2. Table IV listed radiation lengths of a variety of substances. As noted in Section 4, the radiation length is also the important parameter for measuring multiple scattering.

For completeness we shall discuss the radiation of electrons accelerated in a magnetic field, although no experimental use has yet been made of this property.

14.2. *Radiation from Charge Moving in a Magnetic Field*

Electrons deflected by a magnetic field (and thus radially accelerated) radiate energy. We quote results from Schwinger[24] for this process.

The radiated energy E per meter for an electron is given by

$$E_{\text{Mev/meter}} = 1.27\ 10^{-11} H^2_{\text{gauss}} E^2_{\text{Bev}} \tag{113}$$

At 10^4 gauss and 6 Bev this radiation amounts to 47 Kev per meter. These radiated quanta have a spectrum $I'(\nu)\,d\nu$, which goes

as $\nu^{-2/3}\,d\nu$ down to a critical wavelength λ_c, after which very little energy is radiated.

$$\lambda_{c\ \text{angstroms}} = \frac{1.86\ 10^5}{H_{\text{gauss}} E^2_{\text{Bev}}}\ \text{angstroms} \tag{114}$$

for $E = 6$ Bev and $H = 10$ kilogauss, $\lambda_c = 0.5$ angstrom.

The power radiated in the visible region at 6 Bev and 10^4 kilogauss is only a few ev per meter and thus of the order of a few quanta per meter. The radiated energy in the visible region is proportional to $H^{2/3}E^{2/3}$, and becomes less important for constant magnetic field at high energies even though the total radiated power, largely in the form of soft X-rays, is rising rapidly.

14.3. *Compton Scattering of γ-Rays from Free Electrons*

The kinematics of the collisions of γ-rays with free electrons leads to simple results (Fig. 18). As shown in Fig. 18, for a γ-ray incident on an electron at rest, conservation of momentum along the line of flight (Section 12) gives

$$\frac{h\nu}{c} = \frac{h\nu'}{c}\cos\theta_1 + m_e c\sqrt{(\gamma^2 - 1)}\cos\theta_2 \tag{115}$$

Conservation of momentum at right angles to the line of flight gives

$$\frac{h\nu'}{c}\sin\theta_1 = m_e c\sqrt{(\gamma^2 - 1)}\sin\theta_2 \tag{116}$$

and conservation of energy gives

$$h\nu + m_e c^2 = h\nu' + \gamma m_e c^2 \tag{117}$$

Eliminating θ_2 and γ (the angle and energy of the proton) from these three equations, we obtain for the frequency of the scattered quantum,

$$h\nu' = \frac{h\nu m_e c^2}{m_e c^2 + h\nu(1 - \cos\theta_1)} \tag{118}$$

One interesting result of this formula is that for high-energy γ-rays scattered at 90 degrees,

$$h\nu' = \frac{h\nu m_e c^2}{m_e c^2 + h\nu} \approx m_e c^2 \tag{119}$$

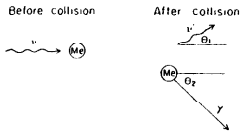

Fig. 18. Differential cross section as a function of the kinetic energy imparted to the electron for various γ energies.

Thus at 90 degrees in the lab the energy of the scattered quantum is ~500 kv and the traverse momentum transfer is $\sim m_e c$, irrespective of the primary energy.

14.4. *Thompson and Klein-Nishina Formulas for Compton Scattering*

At low energies a simple classical treatment gives the correct result for the scattering cross section of γ-radiation. We shall use the Gaussian system of electromagnetic units. If a light wave whose field is represented by the equation

$$\mathcal{E}_x = \mathcal{E}_0 e^{i\omega(t-(z/c))}\epsilon_y = 0 \tag{120}$$

passes by an electron at z_0 the equation of motion of the electron is

$$m_e \frac{d^2x}{dt^2} = -e\mathcal{E}_0 e^{i\omega(t-(z_0/c))}\epsilon_y \tag{121}$$

or

$$\frac{d^2x}{dt^2} = -\frac{e\mathcal{E}_0}{m_e} e^{i\omega(t-(z_0/c))} \tag{122}$$

The energy radiated per second by a classical vibrating charge is given[2] by

$$E = \frac{2}{3}\frac{e^2\langle d\dot{x}^2/dt^2\rangle_{\text{av}}}{c^3} \tag{123}$$

and thus

$$E = \frac{1}{3}\frac{e^4}{m^2c^3}\mathcal{E}_0^2 \tag{124}$$

The incident flux of energy per cm^2 per sec is $c(\mathcal{E}_0^2/8\pi)$ and thus the fraction that is scattered (also the same as the scattering cross

section) is

$$\sigma_{\text{Thomson}} = \frac{8\pi}{3}\left(\frac{e^2}{m_e c^2}\right)^2 = 6.65\ 10^{-25}\ \text{cm}^2 \qquad (125)$$

This treatment is incorrect for energies large compared with the rest mass of the electron. That it is approximately correct at lower energies results from the fact that the transverse momentum transfer is of the same order as the momentum of the incident quantum. The recoiling electron is thus localized within the same radius as the incident γ-ray. At high energies, however, the transverse momentum transfer is $\sim m_e c$, and the recoiling particle is thus localized to $\hbar/m_e c$, whereas the incident quanta is localized in a much smaller radius, $\sim\hbar/p$. It is reasonable to expect this to introduce a "form-factor" effect and decrease the cross section by $\sim m_e c/P$ to give

$$\sigma \approx \sigma_{\text{Thomson}} m_e c/P \qquad (126)$$

The Klein-Nishina formula,[34] asymptotically correct for large energies, is

$$\sigma = \pi\left(\frac{e^2}{mc^2}\right)^2 \frac{m_e c}{h\nu}\left[\log_e\left(\frac{2h\nu}{m_e c}\right) + \frac{1}{2}\right] \qquad (127)$$

This cross section goes almost inversely as the energy of the γ-ray, thus becoming decreasingly important (Fig. 18).[18]

14.5. *Cross-Sectional Absorption of γ-Rays by Pair Production*

High-energy γ-rays incident on nuclei are absorbed and form electron-positron pairs in the electromagnetic field of the nucleus.

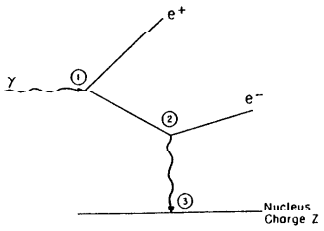

Fig. 19. The absorption of a γ-ray.

A simple order-of-magnitude estimate is provided by the following. We consider a nucleus as being surrounded by virtual positron-electron pairs. Figure 19 shows diagrammatically the absorption of a γ-ray.

Vertices 1 and 2 together are analogous to Thompson scattering and supply a cross section of the order of the Thompson cross section. Vertex 3 puts the process down by a factor of $Z^2e^2/\hbar c$. Thus the total cross section is of the order of $\sigma_{\text{Thompson}}Z^2(e^2/\hbar c)$.

The actual asymptotic total cross section for high energies is given[13] by

$$= \frac{Z^2}{137}\left(\frac{e^2}{mc^2}\right)^2\left[\frac{28}{9}\log_e 183Z^{-1/3} - \frac{2}{27}\right] \qquad (128)$$

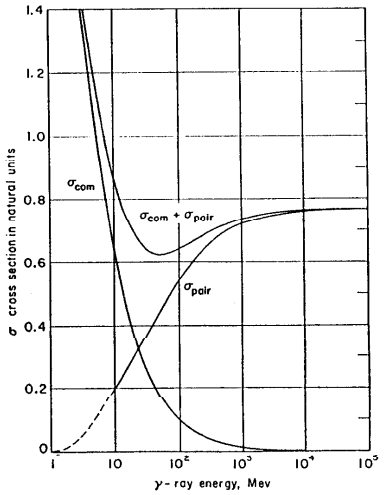

Fig. 20. Pair and Compton cross sections for γ-rays in air. The cross section σ is measured in natural units of $1/NX$ or in units of $4.5\ 10^{-26}$ cm^2 per nucleon.

The cross section is usually expressed in terms of the radiation length, which was defined by Eq. (112):

$$\frac{1}{x} = \frac{4NZ(Z+1)}{137}\left(\frac{e^2}{mc^2}\right)^2 \log_e 183Z^{-1/3}\left[1 + 0.12\left(\frac{Z}{82}\right)^2\right] \quad (129)$$

In these units

$$\sigma_{\text{pair}} \approx \frac{7}{9}\frac{1}{NX_{\text{rad}}} \quad (130)$$

N being the number of atoms per gram and X the radiation length measured in g/cm^2 (Table IV).

The cross section has the following characteristics. The energy dependence is such that for small energies the cross section is zero and rises to its half-value at about 20 Mev, to reach its asymptotic value at about 200 Mev, as shown in Figs. 20 and 21 for air and lead. The distribution of energy between the positron and electron is almost constant per unit energy interval, as shown in Figs. 22 and 23. The recoil momentum of the nucleus is usually small and a fraction of a Mev.[14]

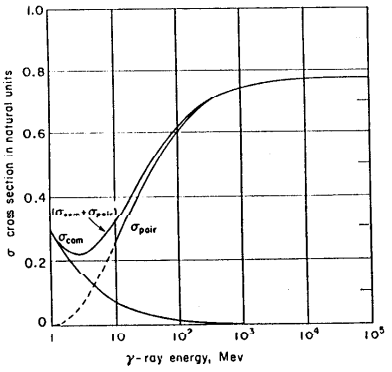

Fig. 21. Pair and Compton cross sections for γ-rays in lead. The cross section σ is measured in natural units of $1/NX$ or in units of 2.6 10^{-25} cm^2 per nucleon.

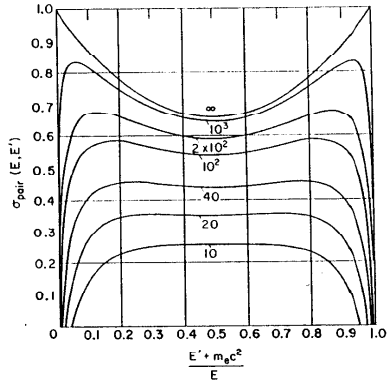

Fig. 22. Differential cross section in air as a function of the energy of the pair electrons for various incident γ-ray energies in natural units.

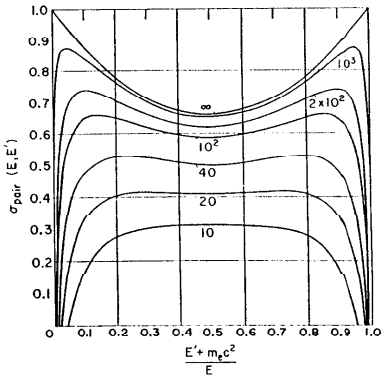

Fig. 23. Differential cross section in lead as a function of energy of the pair electrons for various incident γ-ray energies in natural units.

14.6. *Attenuation of γ-Rays*

The cross section for the absorption of γ-rays is given by Eq. (130) for high-energy γ-rays ($E > 100$ Mev) and by Eq. (125) for low-energy γ-rays ($E > \frac{1}{2}$ Mev).

The Compton scattering cross section decreases with energy, and in addition several collisions are required to remove a γ-ray from the beam. The pair formation cross section only becomes important at higher energies. There is thus in the intermediate region of several Mev a minimum in the total cross section.

The effective mean free path for a γ-ray of several Mev energy is about 70g/cm² for all elements. In a cascade process such as is discussed in Section 16, the final shower products are γ-rays of several Mev which are attenuated comparatively slowly.

Such γ-rays passing through a counter telescope can lose energy in successive counters by Compton scattering and thus simulate the passage of an ionizing particle.

15. Electromagnetic Radiation Processes

15.1. *Cross Section for Bremsstrahlung by Electrons*

The Coulomb fields in matter give very large accelerations to electrons and positrons and they lose much of their energy by radiating quanta. In fact, for electrons with energies above 100 Mev in air and above about 6 Mev in lead this is the dominant process of energy loss.

As in the previous section on pair formation, the process of radiation can be described in terms Fig. 24, which illustrates the

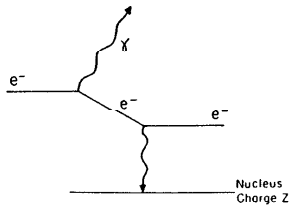

Fig. 24. The process of radiation.

process of radiation. The electron emits a γ-ray and then scatters by exchanging a γ ray with a nucleus.

The diagram is almost identical to that for pair production. The cross section is approximately

$$\sigma(\nu)\, d\nu \approx \sigma_{\text{pair}} \frac{d\nu}{\nu} \approx \frac{z^2}{137}\, \sigma_{\text{Thompson}} \frac{d\nu}{\nu} \tag{131}$$

where ν is the frequency of the radiated quantum.

The exact formula for radiation at relativistic energies is

$$\sigma(E_0 E')dE' = \frac{4Z^2}{137}\left(\frac{e^2}{mc^2}\right)^2 \frac{dE'}{E'} \times \left[1 + \left(1 - \frac{E'}{E_0}\right)^2 - \frac{2}{3}\left(1 - \frac{E'}{E_0}\right)\right] \times \left[\ln 183Z^{-1/3} + \frac{1}{9}\left(1 - \frac{E'}{E_0}\right)\right] \tag{132}$$

where E_0 is the initial energy of the electron and E' is the energy of the radiated quantum.

The average energy loss per g/cm² is found by integrating this formula and is

$$-\frac{dE}{dx} = \frac{4}{137} NZ^2 \left(\frac{e^2}{mc^2}\right)^2 \left[\ln 183Z^{-1/3} + \frac{1}{18}\right] E_0 \tag{133}$$

or

$$-\frac{dE}{dx} \approx \frac{E_0}{X} \tag{134}$$

where X is the radiation length in g/cm².

The differential probabilities for radiating quantum are shown in Figs. 25 and 26 for air and lead. The ordinate is in units of E_0 and the abscissa is the energy in Mev radiated per Mev interval per radiation length traversed. This gives curves which are almost independent of both the material and the energy.

15.2. *"Critical Energy" of Materials*

The critical energy E_c of a material is defined as the energy lost by an electron traversing one radiation unit of material by ionization losses alone. With this definition energy losses by ionization and

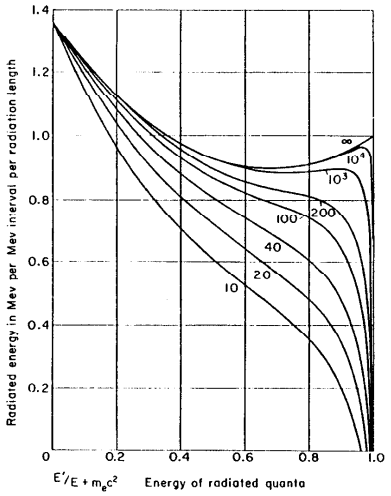

Fig. 25. The energy radiated by an electron in air, in Mev per Mev interval per radiation length traversed. The abscissa is the energy radiated per Mev interval per radiation length, and the ordinate is the radiated γ-ray energy in units of the incident kinetic energy.

radiation are nearly equal at the critical energy. In electromagnetic cascade theory, the approximation is often made that for electron energies above E_c only losses by radiation need be considered and for energies below E_c only collision and ionization losses need be considered. Values of E_c are listed in Table IV. Figure 27 shows collision losses and radiated energy losses.

15.3. *Electron Range Curves and Straggling Errors*

It is apparent from the preceding section that radiation processes are an important and sometimes dominant mechanism for energy loss for electrons in a material. The range-energy curves and range straggling are thus very different from those previously derived for heavier particles.

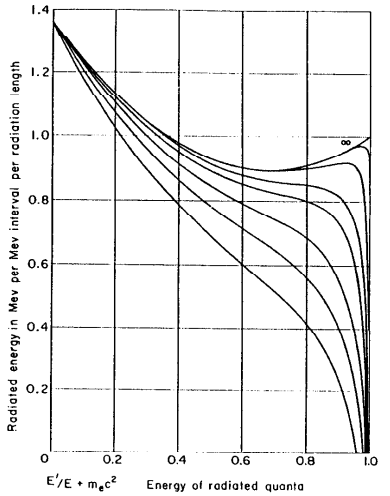

Fig. 26. The energy radiated by an electron in lead, in Mev per Mev interval per radiation length traversed. The abscissa is the radiated energy per Mev per radiation unit, and the ordinate is the radiated γ-ray energy in units of the incident electron kinetic energy.

Wilson[32] has evaluated range curves for electrons by Monte Carlo calculations. Figure 28 shows the mean range and Fig. 29 the percentage straggling for an electron in lead. The percentage straggling of 40 percent is a good approximation for all except the very light elements, and for all energies above about 10 Mev. This arises as follows. At low energies the range is almost linear with energy, and radiation losses, although infrequent, greatly effect the range. At high energies the range depends only logarithmically on energy, and considerable fluctuations in energy loss, although occur-

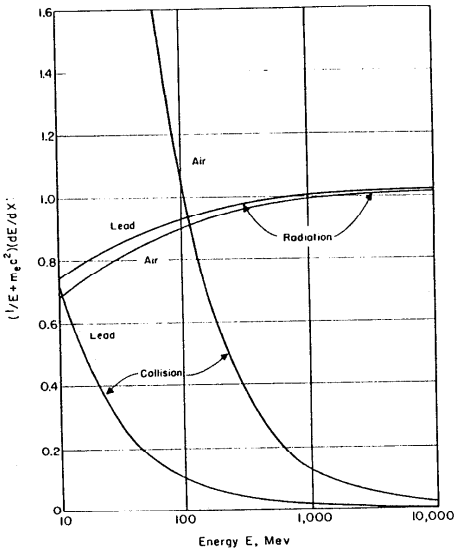

Fig. 27. Collision and radiation losses in air and lead per radiation length as a function of energy.

ring frequently, hardly effect the range. (Range in this context is what would be seen visually as the distance from the beginning to the end of a given track. However, secondary processes, in which γ-rays are emitted and later produce electron-positron pairs and knock-on electrons, are able to penetrate to large distances. Counter setups can sometimes measure spurious ranges due to their inability to distinguish secondary from primary effects.)

16. Electromagnetic Cascade Showers

When an electron or γ-ray passes through matter, the successive radiation of γ-rays and the conversion of these γ-rays into electron-positron pairs gives rise to a multiplicative cascade process.

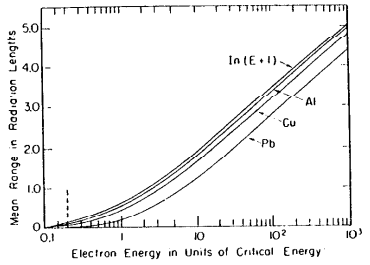

Fig. 28. Mean range of electrons in various materials.

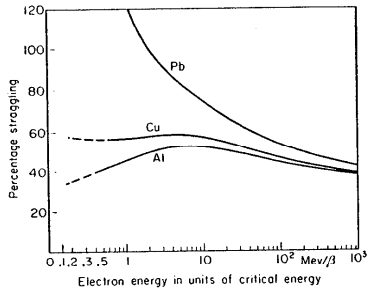

Fig. 29. The rms percentage range straggling $\{[\langle (R - R_0)^2 \rangle^{1/2}]/R_0\} \times 100$ as a function of the electron energy in units of the critical energy for various materials.

Such processes have been evaluated mathematically with asymptotic cross sections. Wilson[33] has, however, made Monte Carlo-type calculations using the correct cross section, and some typical results for electrons and γ-rays are shown in Figs. 30 and 31. In addition, Buttcher and Messel[6] have made accurate Monte Carlo calculations using fast computer techniques.

One obvious result is that all the energy in a shower is eventually dissipated in ionization. Therefore, a measurement of total length

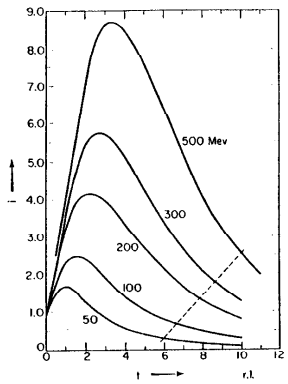

Fig. 30. Ionization in a cascade shower initiated by an electron, in units of the ionization produced by one electron in the beam direction, as a function of depth in lead measured in radiation units for various incident electron energies.

of track and thus of total ionization loss gives the shower energy. However, with a finite-sized apparatus, a fraction of the shower energy escapes from the apparatus in the form of low-energy γ-rays of a few Mev.

Rough rules of thumb can be given for cascade shower behavior.[21] At the shower maximum, the number of particles

$$\approx 0.15 E_0/E_c \log_e \frac{E_0}{E_c}$$

where E_c is the critical energy and E_0 the initial energy. The maximum slower development occurs at a distance of $\log_e (E_0/E_c)^{-1}$ radiation lengths, and the shower at maximum development is spread out over a distance x given by $\langle x^2 \rangle_{av}^{1/2} \approx 0.80\ (E_s/E_c)$ radiation lengths and an angular range θ given by $\langle \theta^2 \rangle_{av}^{1/2} \approx 0.75\ (E_s/E_c)$ radians where $E_s = 21$ Mev.

17. Neutral-Particle Detection

A few properties permit the identification of neutral particles. First, the presence of a magnetic moment leads to ionization losses.

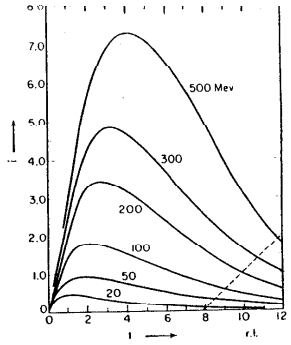

Fig. 31. The average ionization in a cascade shower initiated by a γ-ray, in units of the ionization produced by one electron in the beam direction, as a function of depth in lead measured in radiation units for various incident γ-ray energies.

The amount is, however, negligibly small and has not been experimentally detected. Second, if the particle is unstable it can be detected through its decay process (Section 13) which both characterizes it and measures its energy. An example is the Λ^0-decay into a proton and π^--meson, which gives a readily identifiable signature.

Third, if the neutral particle is known to be a neutron, it can be detected by its interaction with nuclei and the appearance in the subsequent disintegrations of part of its energy as ionization. All the energy in a very large counter can eventually be converted to ionization.

Fourth, in a process such as $\pi^- + p \rightarrow N + \pi^0$ or $N + \gamma$ when the time and place at which the π^- stopped is known, the neutron energy can be determined by measuring its time-of-flight from the stopper to a counter in which it is detected by making a nuclear disintegration.

Fifth, if a neutron collides elastically with a proton, the energy and angle of the recoiling proton determine all the characteristics kinematically (Section 12).

Sixth, threshold detection for neutrons is provided by certain

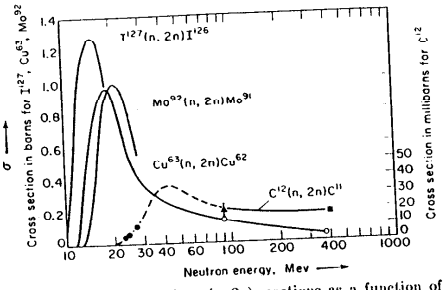

Fig. 32. Cross section for various $(n, 2n)$ reactions as a function of neutron energy.

$(n, 2n)$ reactions. For instance, neutrons of 30 Mev incident on C^{12} form C^{11}, which has a 20-min β^+ decay activity. Figure 32 shows the cross-sectional excitation function for various elements. The neutron fluxes are counted by measuring the β activity after irradiation.

Bibliography

Most laboratories with a high-energy accelerator have handbooks giving the kinematics of processes appropriate to their machine. Particularly useful in this connection are the handbooks from the University of California's Radiation Laboratory. *High Energy Particle Data*, Vols. I and II, are available from the Office of Technical Services, U. S. Department of Commerce, Washington 25, D. C.

Other useful sources include the following:

B. Rossi and K. Greisen, "Cosmic Ray Theory," *Revs. Modern Phys.* **13**, 24 (1941).

B. Rossi, *High Energy Particles*, Chap. I, Prentice Hall, New York

W. Heitler, *Quantum Theory of Radiation*, Clarendon Press, New York, 1951.

H. Bethe and J. Ashkin, *Passage of Radiation through Matter, Experimental Nuclear Physics*, Vol. 1, p. 166, John Wiley, New York.

R. E. Marshak, *Meson Physics (for Kinematic Transformations)*, McGraw-Hill, New York, 1952.

References

1. L. W. Alvarez, H. Bradner, P. FalkVairant, J. D. Gow, A. H. Rosenfeld, F. T. Solmitz, and R. D. Tripp, *Nuovo cimento* **5**, 1026 (1957).

2. M. Abraham and R. Becker, *Classical Theory of Electricity and Magnetism*, Blackie, London, 1950.
3. R. Armenteros, K. H. Barker, C. E. Butler, and A. Cachon, *Phil. Mag.* **42**, 1113 (1951).
4. Aage Bohr, *Kgl. Danske Videnskab. Selskab, Mat.-fys. Medd.* **24**, no. 19 (1948).
5. Hans A. Bethe, *Phys. Rev.* **70**, 821 (1946).
6. J. C. Buttcher and H. Messel, *Report F. B. S. Falkner Nuclear Research and Adolph Basser Computing Lab. Univ. of Sidney*, 1958.
7. W. H. Barkas, P. H. Barrett, P. Cuer, H. Heckman, E. M. Smith, and H. K. Ticho, *Nuovo cimento* **9**, 185 (1958).
8. D. O. Caldwell, *Phys. Rev.* **100**, 291 (1955).
9. E. Fermi, *Phys. Rev.* **57**, 485 (1940).
10. M. Gell-Mann, *Ann. Rev. Nuclear Sci.* **7**, 407 (1957).
11. Y. Goldschmidt-Clermond, *Nuovo cimento* **1**, 220 (1950).
12. J. O. Hirschfelder and E. N. Adams, *Phys. Rev.* **73**, 863 (1948).
13. W. Heitler, *Theory of Radition*, Clarendon Press, New York, 1954.
14. R. Jost, J. M. Luttinger, and M. Slotnick, *Phys. Rev.* **80**, 189 (1950).
15. L. Landau, *J. Phys. (U.S.S.R.)* **4**, no. 8, 201 (1944).
16. G. Moliere, *Z. Naturforsch.* **3**, 78 (1948).
17. N. F. Mott and H. S. W. Massey, *The Theory of Atomic Collisions*, 2nd ed., Clarendon Press, New York, 1949.
18. A. T. Neams, "Graphs of the Compton Energy Angle Relationship and the Klein-Nishina Formula from 50 Kev to 500 Mev," *National Bureau of Standards Circular 542*, pp. 1–89, 1953.
19. W. Pauli, *Revs. Modern Phys.* **13**, 203 (1941).
20. W. K. Panofsky, R. Aamodt, and J. Haddley, *Phys. Rev.* **81**, 565 (1951).
21. B. Rossi and K. Greisen, *Revs. Modern Phys.* **13**, 240 (1941).
22. B. Rossi, *High Energy Particles*, Prentice-Hall, New York, 1952.
23. M. Rich and R. Madey, "Range-Energy Tables," *UCRL 2301*, 1954.
24. J. Schwinger, *Phys. Rev.* **75**, 1912 (1949).
25. J. Steinberger, W. H. Panofsky, and J. Steller, *Phys. Rev.* **78**, 802 (1950).
26. K. R. Symons, *Harvard University Thesis*, 1948.
27. R. M. Sternheimer, *Phys. Rev.* **103**, 511 (1956).
28. R. W. Thompson, *Prog. Cosmic Ray Physics*, **III**, 255 (1956).
29. L. Voyvodic and E. Pickup, *Phys. Rev.* **85**, 91 (1952).
30. E. J. Williams, *Proc. Roy. Soc. (London)* **169**, 531 (1939).
31. E. J. Williams, *Revs. Modern Phys.* **17**, 217 (1945).
32. R. R. Wilson, *Phys. Rev.* **84**, 100 (1951).
33. R. R. Wilson, *Phys. Rev.* **86**, 261 (1952).